Aerosol Synthesis of Anatase Titanium Dioxide Nanoparticles for Hybrid Solar Cells

Carolien L. Huisman,* Albert Goossens, and Joop Schoonman

Laboratory for Inorganic Chemistry, Faculty of Applied Sciences, Delft University of Technology, Julianalaan 136, 2628 BL, Delft, The Netherlands

Received June 23, 2003. Revised Manuscript Received September 8, 2003

Using an aerosol technique, in which ultrasonically formed droplets of titanium isopropoxide are pyrolyzed, thin films of nanosized anatase titanium dioxide (TiO_2) particles are deposited. The size of the particles and the morphology of the films depend on the deposition parameters, i.e., reaction temperature, concentration of the precursor, and gas flow. Under optimal conditions, films can be deposited which consist of stoichiometric anatase TiO_2 particles with diameters of 50−300 nm. With these films, solar cells are constructed by spin casting poly(3-octyl)thiophene (P3OT) on top. Devices with a 1-μm film of porous TiO_2 and P3OT inside the pores have a short circuit current (I_{sc}) of 0.25 mA/cm^2, an open circuit voltage (V_{oc}) of 0.72 V, a fill factor (FF) of 0.35, and an efficiency (η) of 0.06% under white light illumination (1000 W/m^2). The efficiency is a factor of 20 higher than that of cells based on flat films of anatase TiO_2, whereas the OD for both systems is comparable (flat film equivalent of 60-nm P3OT). The incident photon to current efficiency (IPCE) for the nanostructured solar cell is 2.5% at 488 nm. Devices prepared by adding P3OT during the deposition of the porous TiO_2 show the same performance as the cells where P3OT is applied after TiO_2 deposition. This shows that penetration of the polymer is quite effective in this system. It is found that P3OT can penetrate these porous TiO_2 films as deep as 1 μm.

Introduction

Titanium dioxide is a key chemical and has attracted a lot of interest for optical and optoelectronic applications.[1] In 1991 O'Regan and Grätzel showed that a solar cell comprising a porous layer of anatase TiO_2 particles of 15 nm in combination with a sensitizing ruthenium complex and a liquid electrolyte exhibits an energy conversion efficiency of 8%.[2] At present, these cells have an efficiency of around 10%.[3] However, the presence of a liquid electrolyte in the system is a major bottleneck for further development, as time- and money-consuming sealing has to be applied to prevent leakage.

Several attempts have been undertaken to design dye-sensitized solar cells excluding the liquid electrolyte.[4] It can be replaced by an ion-conducting polymer[5−7] or hole-conducting material.[8,9] Another possibility is to use organic or inorganic compounds that do not only absorb visible light and inject electrons into TiO_2, but also transport the holes to the back contact. In this concept the pores in nanostructured TiO_2 are filled with a visible light-absorbing and hole-conducting material.[10−15] A problem in constructing these cells is the necessity of a high-temperature sintering step to obtain good-quality nanostructured anatase titania films. Most organic dyes are not stable at these temperatures and can only be applied afterward. This is a problem when bulky molecules have to penetrate into the nanosized pores. Uniaxial pressing of nc-TiO_2 films could open up a way to avoid the sintering step, making it possible to blend the organic phase with the TiO_2 particles beforehand.[16,17] Synthesizing a network of TiO_2 and organic dye at the same time would be an elegant solution to this dilemma, leading to a high interfacial area and intimate contact between the components.[18]

* Corresponding author. Tel: +31 152782637. Fax: +31 152788047. E-mail: C.L.Huisman@tnw.tudelft.nl.

(1) Grätzel, M. *Nature* **2001**, *414*, 338−358.
(2) O'Regan, B.; Grätzel, M. *Nature* **1991**, *353*, 737−740.
(3) Nazeerudddin, M.-K.; Kay, A.; Rodicio, I.; Humphry-Baker, R.; Müller, E.; Liska, P.; Vlachopoulos, N.; Grätzel, M. *J. Am. Chem. Soc.* **1993**, *115*, 6328.
(4) Nelson, J. *Curr. Opin. Solid State Mater. Sci.* **2002**, *6*, 87−95.
(5) Cao, F.; Oskam, G.; Searson, P. C. *J. Phys. Chem.* **1995**, *99*, 17071−17073.
(6) Nogueira, A. F.; De Paoli, M.-A. *Sol. Energy Mater. Sol. Cell* **2000**, *61*, 135−141.
(7) Nogueira, A. F.; Durrant, J. R.; De Paoli, M.-A. *Adv. Mater.* **2001**, *13*, 826−830.
(8) Bach, U.; Lupo, D.; Compte, P.; Moser, J. E.; Weissörtel, F.; Salbeck, J.; Spreitzer, H.; Grätzel, M. *Nature* **1998**, *395*, 583−585.
(9) Krüger, J.; Plass, R.; Cevey, L.; Piccirelli, M.; Grätzel, M. *Appl. Phys. Lett.* **2001**, *79*, 2085−2087.
(10) Kaneko, M.; Takayama, K.; Pandey, S. S.; Takashima, W.; Endo, T.; Rikukawa, M.; Kaneto, K. *Synth. Met.* **2001**, *121*, 1537−1538.
(11) Tennakone, K.; Kumara, G. R. R. A.; Kumarasinghe, A. R.; Wijayantha, K. G. U.; Sirimanne, P. M. *Semicond. Sci. Technol.* **1995**, *10*, 1689−1693.
(12) Salafsky, J. S. *Solid-State Electron.* **2001**, *45*, 53−58.
(13) Breeze, A. J.; Schlesinger, Z.; Carter, S. A. *Phys. Rev. B* **2001**, *64*, 125205-1−125205-9.
(14) Arango, A. C.; Carter, S. A.; Brock, P. J. *Appl. Phys. Lett.* **1999**, *74*, 1698−1700.
(15) Gebeyehu, D.; Brabec, C. J.; Padinger, F.; Fromherz, T.; Spiekermann, S.; Vlachopoulos, N.; Kienberger, F.; Schindler, H.; Saricifici, N. S. *Synth. Met.* **2001**, *121*, 1549−1550.
(16) Lindström, H.; Magnusson, E.; Holmberg, A.; Södergren, S.; Lindquist, S.-E.; Hagfeldt, A. *Sol. Energy Mater. Sol. Cell* **2002**, *73*, 91−101.
(17) O'Regan, B.; Lenzmann, F.; Muis, R.; Wienke, J. *Chem. Mater.* **2002**, *14*, 5023−5029.
(18) Van Hal, P. A.; Wienk, M. M.; Kroon, J. M.; Verhees, W. J. H.; Slooff, L. H.; van Gennip, W. J. H.; Jonkheijm, P.; Janssen, R. A. J. *Adv. Mater.* **2003**, *15*, 118−121.

10.1021/cm031099m CCC: $25.00
Published on Web 11/06/2003

In this paper we report on a route to synthesize nanostructured anatase TiO_2 films in which a sintering step after deposition is not necessary. Using ultrasonically generated aerosols of a TiO_2 precursor, films of nanoparticles can be formed in a controlled way in ambient atmosphere. It is shown that these films can be used in solar cells. After spin coating poly(3-octyl)-thiophene on top of these porous TiO_2 films, solar cells are obtained. It is shown that enlargement of the interfacial area improves the conversion efficiency. It is also possible to add polymer to the film during deposition, yielding TiO_2/P3OT interpenetrating networks in one step.

Polythiophenes are relatively stable in ambient atmosphere and under illumination in comparison to, for example, poly vinylene phenylenes (PPVs). The band gap, position of the conduction band, and hole mobility make them interesting candidates for solar cells. For successful application in solar cells, the distance that both excitons and holes have to travel must be kept as small as possible, as the exciton diffusion length is only 3−5 nm in regioregular P3OT.[19,20] There have been a number of reports on heterojunctions of TiO_2 and oligo- or polythiophenes.[10,21−31] Recently, a bulk heterojunction of CdSe nanorods and poly(3-hexylthiophene) was reported to have an efficiency of 1.7% under AM 1.5 conditions.[21]

Experimental Section

The employed aerosol synthesis technique for nanosized TiO_2 particles is known in the literature under a variety of names including aerosol decomposition, spray roasting, and spray pyrolysis.[32−36] Figure 1 shows the setup for aerosol synthesis of nanocrystalline TiO_2 particles. It comprises a commercial ultrasonic nebulizer (oscillating frequency 1.63 MHz) in which a diluted precursor solution is agitated to form small droplets. As precursor titanium isopropoxide (TTIP, Aldrich 98%+) diluted with absolute ethanol is used, kept at a constant temperature of 40 °C. Part of the as-formed aerosol is transported along with an argon carrier flow through a quartz tube, which passes a furnace at the end. The temperature inside the furnace is measured with a thermocouple. A flow of oxygen is added just before the furnace. When the droplets of the titanium precursor solution travel through the furnace, they are pyrolyzed to form TiO_2 particles, which are subsequently deposited on a horizontal substrate placed at the exhaust of the tube. The substrate is attached to a spin-coater, which is rotating at 3000 rpm. As substrate material fluor-doped SnO_2 is used (Transparent Conducting Oxide, Libbey Owens Ford, 20 Ω/cm). Substrates are thoroughly cleaned in an ultrasonic bath with ethanol and acetone successively and are dried in a nitrogen stream. Most substrates are covered with a thin dense film of anatase TiO_2 (70 nm, deposited by spray pyrolysis) prior to deposition of the nanocrystalline TiO_2 particles.[37] This film serves as a selective contact, preventing short-circuiting.

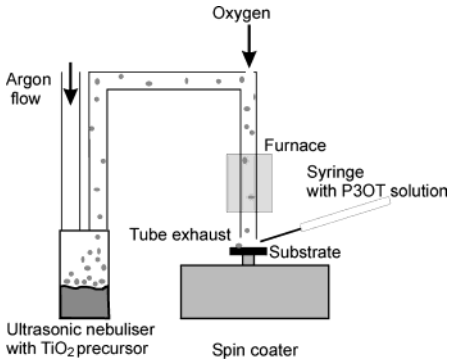

Figure 1. Setup for synthesis of TiO_2 particles using an ultrasonically generated aerosol.

On top of the TiO_2 films, a solution of poly(3-octyl)thiophene (Aldrich, regioregular) is spin-coated. The polymer is used without additional purification. A solution of 5−20 mg/mL in chloroform is freshly prepared and ca. 5 drops are applied to the substrate until the whole surface is covered with a solution layer. Subsequently, the substrate is spinned at 1500 rpm for 20 s, leading to a polymer film with the same optical density (OD) as an equivalent film of 30−115 nm (depending on the concentration) deposited on a flat substrate. After spin coating of P3OT, the samples are annealed for $^1/_2$ hour at 100 °C to remove remaining chloroform. For the samples that are prepared in one step, the P3OT solution is added dropwise from a syringe during the aerosol deposition of nc-TiO_2. The number of drops that are added, the concentration of the solution, and the interval are varied.

The crystal structure of the films is studied with grazing incidence X-ray diffraction by using a Bruker D8 Advance X-ray diffractometer. Raman spectra are recorded on a home-built setup, using a SpectraPhysics Millenia Nd:YVO_4 laser with a wavelength of 532 nm. Raman scattering is recorded in the backscattering mode, using a set of notch filters to remove Raleigh scattering, a liquid-nitrogen-cooled CCD camera (Princeton Instruments LN/CCD-1100PB), and a Spex 340E monochromator equipped with a 1800 grooves/mm grating. The morphology and layer thickness are studied with (high-resolution) scanning electron microscopy using a JEOL JSM-5800 LV scanning electron microscope (SEM) and a JEOL JSM 6500 F field emission SEM (high-resolution SEM).

Current−voltage characteristics and wavelength-dependent photocurrent spectra are recorded using a Keithley 2400 digital source meter. A 250 W tungsten−halogen lamp in combination with an Acton Spectra-Pro-275 monochromator is used to illuminate the samples through the TCO substrate with an intensity of 100 mW/cm^2 in the case of white light, and with ca. 2 mW/cm^2 in the case of monochromatic light. A 360-nm

(19) Pettersson, L. A. A.; Roman, L. S.; Inganas, O. *J. Appl. Phys.* **1999**, *86*, 487−496.
(20) Theander, M.; Yartsev, A.; Zigmantas, D.; Sundstrom, V.; Mammo, W.; Andersson, M. R.; Inganas, O. *Phys. Rev. B* **2000**, *61*, 12957−12963.
(21) Huynh, W. U.; Dittmer, J. J.; Alivisatos, A. P. *Science* **2002**, *295*, 2425−2427.
(22) Noma, N.; Tsuzuki, T.; Shirota, Y. *Adv. Mater.* **1995**, *7*, 647−648.
(23) Sicot, L.; Geffroy, B.; Lorin, A.; Raimond, P.; Sentein, C.; Nunzi, J.-M. *J. Appl. Phys.* **2001**, *90*, 1047−1054.
(24) Smestad, G. P.; Spiekermann, S.; Kowalik, J.; Grant, C. D.; Schwartzberg, A. M.; Zhang, J.; Tolbert, L. M.; Moons, E. *Sol. Energy Mater. Sol. Cell* **2003**, *76*, 85−105.
(25) Videlot, C.; Fichou, D. *Synth. Met.* **1999**, *102*, 885−888.
(26) Videlot, C.; Fichou, D.; Garnier, F. *Synth. Met.* **1999**, *101*, 618−619.
(27) Videlot, C.; Ackermann, J.; El Kassmi, A.; Raynal, P. *Thin Solid Films* **2002**, *403−404*, 380−383.
(28) Song, M. Y.; Kim, J. K.; Kim, K.-J.; Kim, D. Y. *Synth. Met.* **2003**, *137*, 1389−1390.
(29) Ding, H.; Ram, M. K.; Nicolini, C. *J. Mater. Chem.* **2002**, *12*, 3585−3590.
(30) Kim, Y. G.; Walker, J.; Samuelson, L. A.; Kumar, J. *Nano Lett.* **2003**, *3*, 523−525.
(31) Ding, H.; Ram, M. K.; Nicolini, C. *J. Nanosci. Nanotechnol.* **2001**, *1*, 207−213.
(32) Lyons, S. W.; Ortega, J.; Wang, L. M.; Kodas, T. T. *Mater. Res. Soc. Symp. Proc.* **1992**, *271*, 907−917.
(33) Ogihara, T.; Ookura, T.; Yanagawa, T.; Ogata, N.; Yoshida, K. *J. Mater. Chem.* **1991**, *1*, 789−794.
(34) Zhang, S. Z.; Messing, G. L. *J. Am. Ceram. Soc.* **1990**, *73*, 67.
(35) Dubois, B.; Ruffier, D.; Odier, P. *J. Am. Ceram. Soc.* **1989**, *72*, 713−715.
(36) Ahonen, P. P.; Tapper, U.; Kauppinen, E. I.; Joubert, J.-C.; Deschanvres, J.-L. *Mater. Sci. Eng.* **2001**, *A315*, 113−121.
(37) Paraguay, F. D.; Estrada, W. L.; Acosta, D. R. N.; Andrade, E. M.; Miki-Yoshida, M. *Thin Solid Films* **1999**, *350*, 192−202.

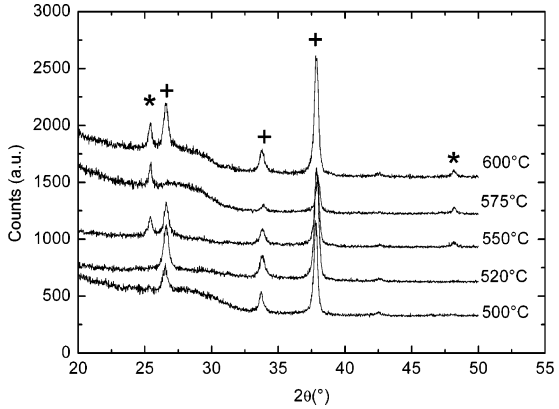

Figure 2. Grazing incidence X-ray diffraction patterns of nanocrystalline TiO_2 for different furnace temperatures. The crosses denote the tin dioxide peaks; the asterisks denote the anatase peaks. The spectra are offset for clarity.

high-pass filter is used for the wavelength-dependent photocurrent spectra and a 400-nm high pass filter is used to remove UV-light during the measurements under white light illumination. As back contacts evaporated gold contacts with a diameter of 2 mm and a thickness of 50 nm are used. Contact to the contacts is made with a gold-coated tip, attached to a spring with a spring constant of 7×10^{-3} Nm^{-1} (Ingun Prüfmittelbau GmbH). Some measurements are carried out using a mercury back contact, yielding the same results as for gold. Measurements are performed in ambient atmosphere and at room temperature. Care is taken to measure samples directly after the polythiophene film is spin-coated and to avoid exposure to light, as this is known to cause degradation of semiconducting polymers.[38,39]

For comparison, some devices are prepared using a nc-TiO_2 film formed from commercially available TiO_2 powder. Films are made consisting of either Solaronix HT paste (average particle size 9 nm, thickness of the film 300 nm and 1 μm) or a 50-nm particle size paste, prepared by a sol−gel method (thickness of the film 50 nm and 2 μm). On top of all these nc-TiO_2 films, P3OT is spin-coated from a 10 mg/mL solution in chloroform, leading to an amount of polymer in the pores with the same OD as an equivalent flat film of 60 nm.

Results and Discussion

Preparation of Nanoporous TiO_2. To study the influence on the structure and the morphology of the TiO_2 particles, the following process parameters are systematically varied: the concentration of TTIP in the precursor solution, the distance between tube exhaust and substrate, the temperature of the furnace, the flow of argon, and the flow of oxygen.

In Figure 2 grazing incidence X-ray diffraction patterns are shown of TiO_2 films produced with the aerosol technique at different furnace temperatures. Below 550 °C, only peaks originating from the tin dioxide substrate are present; the TiO_2 film is amorphous. At temperatures above 550 °C, additional peaks appear, which can be assigned to the anatase phase of titanium dioxide. The temperature at which anatase is formed in these experiments is much higher than, for example, in chemical vapor deposition of TiO_2, where anatase already forms at 300 °C.[40−42] This apparent increase in anatase formation temperature is caused by the short residence time of the precursor droplets in the furnace (typically less than a second). In this short period, the vapor is not fully heated to the temperature of the furnace. Only when the furnace temperature is sufficiently high, complete thermolyis of TTIP to anatase TiO_2 does take place. To check for the presence of possible minor fractions of other phases, which cannot be detected by XRD, Raman measurements are performed. In Figure 3 Raman spectra are shown for TiO_2 deposited at different furnace temperatures. Again, it is clear that at temperatures lower than 550 °C the TiO_2 formed is amorphous, whereas above 550 °C the particles exhibit the anatase structure.[43] No other phases are detected, but it is possible that a small amorphous fraction is present in the films, because this would not be visible in either Raman or XRD.

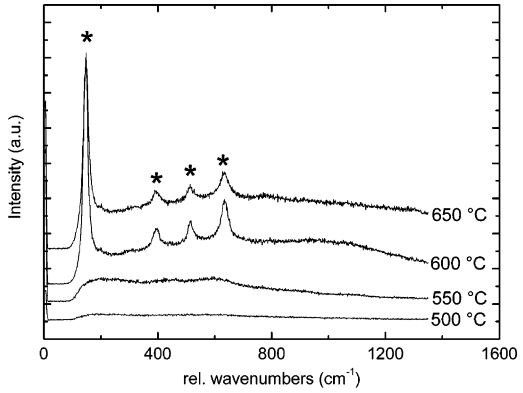

Figure 3. Raman spectra of nanocrystalline TiO_2 for different deposition temperatures. The asterisks denote the anatase peaks. The spectra are offset for clarity.

Using (HR)SEM the morphology of the TiO_2 layers is studied. Figure 4A shows a SEM micrograph of anatase particles, deposited at a furnace temperature of 550 °C, with 100% TTIP as precursor, distance between tube exhaust-to-sample distance 2 cm, oxygen flow of 13 L/h, and argon flow of 20 L/h. The particles are spherical and the size distribution ranges from 50 nm to 1 μm. Figure 4B shows a detailed HRSEM recording of a TiO_2 film, deposited at a furnace temperature of 640 °C, with 5% TTIP in ethanol as precursor, distance between tube exhaust-to-sample distance 0.5 cm, oxygen flow of 53 L/h, and argon flow of 1.1 L/h. The particle size distribution is now much smaller, ranging from 50 to 300 nm. The pores between the particles are about 30 nm in diameter. It is found that at higher precursor dilution and with a smaller argon flow, the size dispersion decreases. This can be explained by the fact that the smallest particles are formed from one single droplet of precursor solution. Part of the precursor droplets fuse before pyrolysis takes place, leading to larger particles. Lower carrier gas flows and a more diluted solution yield a smaller concentration of droplets and, therefore, a more homogeneous particle size distribution with a higher fraction of the smallest particles.

In Figure 5 SEM micrographs are shown for samples obtained with different process parameters. If the

(38) Van der Zanden, B.; Goossens, A.; Schoonman, J. *Synth. Met.* **2001**, *121*, 1601−1602.
(39) Fichou, D., Ed. *Handbook of Oligo- and Polythiophenes*; Wiley-VCH: Weinheim, 1999.
(40) Wu, Y.-M.; Bradley, D. C.; Nix, R. M. *Appl. Surf. Sci.* **1993**, *64*, 21−28.
(41) Fitzgibbons, E. T.; Sladek, K. J.; Hartwig, W. H. *J. Electrochem. Soc.* **1972**, *119*, 735−739.
(42) Boschloo, G. K.; Goossens, A.; Schoonman, J. *J. Electrochem. Soc.* **1997**, *144*, 1311−1317.
(43) Parker, J. C.; Siegel, R. W. *J. Mater. Res.* **1990**, *5*, 1246−1252.

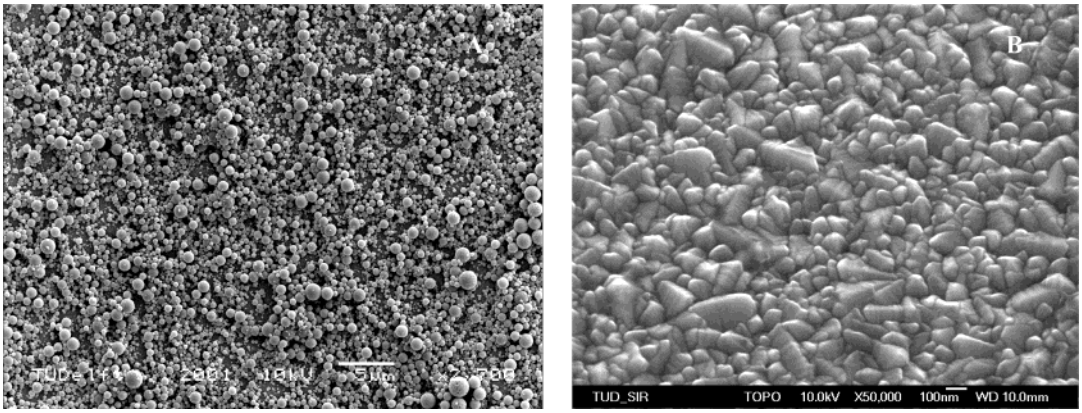

Figure 4. (A) SEM micrograph of TiO_2 particles deposited with a furnace temperature of 550 °C, 100% TTIP as precursor, a distance from tube to sample of 2 cm, an oxygen flow of 13 L/h, and an argon flow of 20 L/h. The length of the scale-bar is 5 μm. (B) HRSEM recording of TiO_2 particles, deposited on SnO_2:F with a furnace temperature of 640 °C, 5% TTIP in ethanol as precursor, a distance from tube to sample of 0.5 cm, an oxygen flow of 10 L/h, and an argon flow of 1.1 L/h.

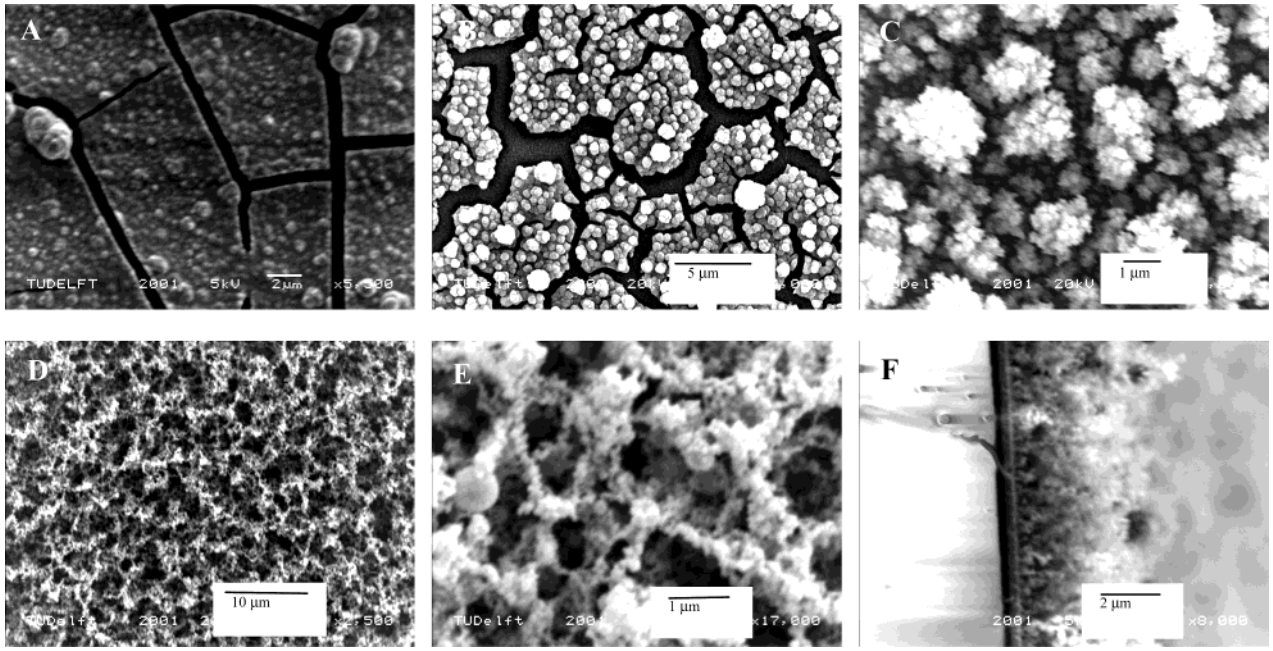

Figure 5. Scanning electron micrographs of TiO_2 particles, deposited on SnO_2:F with different process parameters. Middle of the sample (A), halfway between center and edge (B), at the edge (C). TiO_2 networks are formed for thicker samples (D, E). Cross-section of a thick film (F).

distance between tube exhaust and substrate is small (0.5 cm), sintering between the TiO_2 particles occurs as a result of the hot gas flow. Exactly beneath the tube exhaust, where the temperature is highest, an almost smooth layer develops in which the individual particles are hardly visible anymore (Figure 5A). More to the edges of the sample, the particles are still present, but they form large agglomerates with cracks between them (Figure 5B). These cracks are probably stress-induced and are caused by the fast cooling rate after deposition. At the edge of the sample, the temperature is low enough to prevent sintering (Figure 5C). If the distance between the tube exhaust and the substrate is increased, no sintering is observed (see Figure 4A for a distance of 2 cm). Although the temperature of the substrate is not monitored, an estimated temperature of about 100 °C can be reached if the distance between tube exhaust and substrate is 0.5 cm, whereas the temperature stays below 50 °C if the distance is increased to 2 cm. Locally much higher temperatures can be reached which explains the observed sintering of the particles. Although extensive sintering is detrimental for the morphology of the TiO_2 film, we have reason to believe that a certain increase of substrate temperature is beneficial for the creation of a well-conducting TiO_2 network, as it allows the formation of necks between the individual particles. To prevent degradation of the polymer in the experiments where devices are prepared by adding P3OT during TiO_2 deposition, a "cool-down" time of 30 s is introduced before P3OT solution droplets are added. No color change is observed for the samples that are prepared during TiO_2 deposition as compared to the samples that are prepared by postdeposition addition of P3OT, indicating that major degradation is not occurring.

At prolonged deposition times a thick, porous network is formed (Figure 5D−F). Substrates become opaque and the film can be removed rather easily by brushing it gently with a tissue.

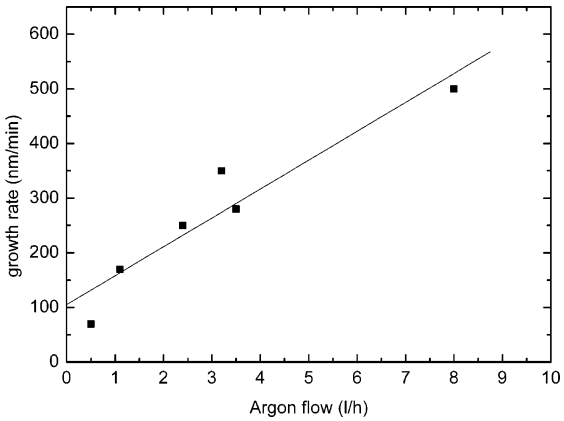

Figure 6. Growth rate of nc-TiO_2 films as a function of argon carrier gas flow. The distance between tube exhaust and substrate is kept constant at 2 cm. The oxygen flow is 10 L/h. The concentration of TTIP in the precursor solution is 5%, kept at a constant temperature of 40 °C. The temperature of the furnace is kept constant at 630 °C. The solid line is a linear fit to the data points.

Table 1. Optimal Process Parameters[a] for Thin Films of nc-TiO_2

furnace temperature	640 °C
TTIP concentration	5% in ethanol
distance tube exhaust to substrate	1 cm
oxygen flow	53 L/h
argon flow	1.1 L/h

[a] These parameters are used for the deposition of TiO_2 films to make devices with poly(3-octyl)thiophene.

If TiO_2 particles are deposited without additional oxygen the films become gray. This is caused by the presence of oxygen vacancies compensated by conduction-band electrons and the product is best described as TiO_{2-x}. Supplying a flow of oxygen to the tube leads to the formation of stoichiometric TiO_2 films that appear to be white. Thick films (more than 2 μm) appear opaque, but thinner films are transparent. The effect of additional oxygen on the solar cell characteristics will be discussed in more detail later.

By measuring the thickness of cross-sections of TiO_2 films deposited with different argon flow rates, it is possible to determine the growth rate as a function of argon flow. A graph of this relationship is shown in Figure 6. The growth rate is roughly linearly dependent on the flow rate. The growth rate increases when the distance between tube exhaust and substrate is decreased. With a typical argon flow of 1 L/h and a distance of 2 cm, films are deposited at about 200 nm/min. As shown in Figure 6, the linear fit does not pass the origin. At zero argon flow, a small growth-rate remains, due to diffusion of TTIP droplets.

In Table 1 the optimal process parameters for the deposition of stoichiometric anatase TiO_2 particles with a homogeneous particle size distribution are summarized. In short, we find that the distance between tube exhaust and sample must be large enough to prevent extensive sintering but small enough to form interconnected TiO_2 particles. The supply of additional oxygen is necessary to prevent the formation of oxygen vacancies. The temperature of the furnace should be higher than 550 °C to obtain anatase TiO_2. The argon carrier flow rate determines the growth-rate and the size distribution, whereas the concentration of the precursor also influences the latter. The values given in Table 1 are used to deposit films for the devices with poly(3-octyl)thiophene.

Devices with Poly(3-octyl)thiophene. Electrical and photovoltaic properties of devices of TiO_2 and polymer are investigated. These cells are prepared by spin-coating a P3OT solution either during or after deposition.

In literature, dye-sensitized solar cells contain TiO_2 particles with a size around 15 nm.[44] But to allow polythiophene to penetrate into a TiO_2 film, the pore diameters should not be too small. Furthermore, a maximum penetration depth of spin-coated polymer is expected, leading to an optimal thickness for the TiO_2 layer. In the remainder of this paper, we will investigate the relation between pore size, penetration depth, and photovoltaic properties in more detail. The size of the particles and the pores shown in Figure 5 is about 50 nm.

First, cells are investigated that consist of nc-TiO_2 on which P3OT is spin-coated after deposition. The thickness of the nc-TiO_2 film is varied and current−voltage characteristics are recorded in the dark and under illumination. In Figure 7A, the photocurrent at 0 V (I_{sc}; short circuit current) is plotted as a function of deposition time for two different distances between tube exhaust and substrate. When converted into film thicknesses (using the calculated growth rate), it is clear that the maximum of the photocurrent is reached at a TiO_2 film thickness of approximately 1 μm for both exhaust-to-sample distances (Figure 7B). Furthermore, it is observed that the maximum is higher at a smaller tube exhaust to substrate distance. This is probably caused by an increase of the substrate temperature for smaller tube exhaust to substrate distances leading to an improved contact between the TiO_2 particles. At distances that are too small, the particles sinter completely and nanostructured film is no longer formed (vide infra).

To find the optimum flow of oxygen in the deposition process, devices are prepared under the same conditions while the oxygen flow rate is varied. In Figure 8 the short circuit current of the TCO/TiO_2/nc-TiO_2/P3OT/Au cells is plotted as a function of the oxygen flow. For low oxygen flows the photocurrent increases linearly with the amount of oxygen, whereas it levels off at flow rates around 50 L/h. Therefore, this oxygen flow rate is chosen for all TiO_2 film depositions (see Table 1).

Other devices are prepared by adding P3OT during the deposition of the porous TiO_2 while systematically varying the process parameters. In Table 2 photovoltaic characteristics are summarized for a number of devices. As can be seen, these cells yield at maximum about the same photovoltaic characteristics as postdeposition spincasting of P3OT. This indicates that the penetration of P3OT occurs quite effectively in this porous system.

To investigate in more detail the penetration of poly(3-octyl)thiophene into a nanoporous network of TiO_2, experiments without selective contacts are carried out. When an interpenetrating film of TiO_2/P3OT (spin-coated after nc-TiO_2 deposition) mixture is sandwiched between TCO and Au two situations can be distin-

(44) Barbé, C. J.; Arendse, F.; Comte, P.; Jirousek, M.; Lenzmann, F.; Shklover, V.; Grätzel, M. *J. Am. Chem. Soc.* **1997**, *80*, 33157−3171.

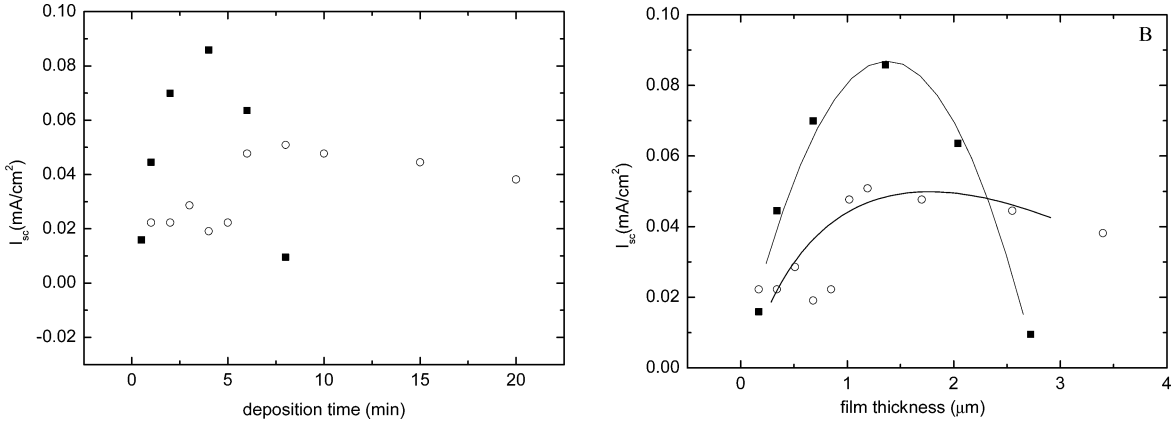

Figure 7. Short circuit current of TCO/TiO_2 (dense, <100 nm)/nc-TiO_2/P3OT as a function of the thickness of the nc-TiO_2 layer for two different distances between tube exhaust and substrate. P3OT is spin-coated after deposition of the nc-TiO_2 film. See Table 1 for deposition parameters. Illumination with white light (100 mW/cm^2, not AM 1.5, 400-nm high pass filter to remove UV-light) takes place through the tin dioxide electrode. (A) I_{sc} plotted versus deposition time. The distance from tube exhaust to substrate is 1 cm (filled squares) or 2 cm (open circles). (B) I_{sc} plotted after conversion to thickness of the TiO_2 layer, using the growth rate for the two distances. The lines are drawn as guide for the eye.

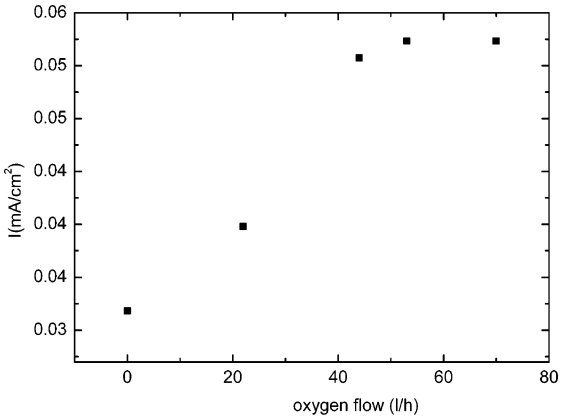

Figure 8. Short circuit current, I_{sc}, of TCO/TiO_2 (dense, <100 nm)/nc-TiO_2/P3OT devices as a function of oxygen flow. See Table 1 for deposition parameters of the TiO_2 particles. Illumination with white light (100 mW/cm^2 and a 400-nm high pass filter to remove UV-light) takes place through the tin dioxide electrode.

Table 2. Devices Prepared by Dropwise Addition of P3OT during TiO_2 Deposition[a]

P3OT conc. (mg/mL)	number of drops	interval between drops (s)	film thickness (μm)	I_{sc} (mA/cm^2)	V_{oc} (V)
2.5	1	90	1	0.15	0.45
2.5	1	60	1	0.099	0.7
2.5	1	40	1	0.048	0.6
2.5	1	20	1	0.012	0.3
2.5	1	10	0.2	0.041	0.25
2.5	1	5	0.2	0.038	0.2
1	1	40	1	0.13	0.2
1	1	20	1	0.14	0.55
1	1	10	1	0.16	0.35
1	3	90	1	0.025	0.2
1	3	30	1	0.0096	0.2
1	3	20	1	0.019	0.2
1	3	10	1	0.035	0.4

[a] For TiO_2 deposition parameters see Table 1.

guished. In the first case, the nc-TiO_2 film is thin enough for the P3OT to penetrate completely from top to bottom (Figure 9A). P3OT makes an ohmic contact to both TCO and gold contacts, and a linear I−V graph, with the reciprocal of the resistance of the P3OT film as slope, is observed when the voltage is scanned. In the second

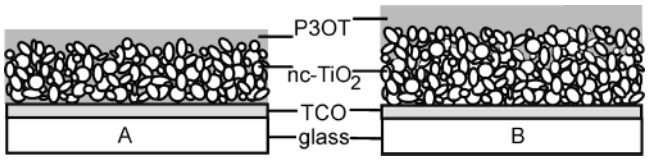

Figure 9. Schematic overview of penetration of P3OT in nc-TiO_2. (A) P3OT penetrates completely to bottom of the nc-TiO_2 film; (B) P3OT partly penetrates the nc-TiO_2 film.

case, the nc-TiO_2 film is too thick for the P3OT to reach the bottom (Figure 9B). Hence, a clear interface between TiO_2 and P3OT will be present at some location in the film and a diode-type I−V characteristic is observed. For different thicknesses of the nanoporous TiO_2 film I−V curves are recorded of TCO/nc-TiO_2/P3OT/Au devices with a spin-coated P3OT layer (10 mg/mL, leading to a flat film equivalence of about 60 nm) on top of the nc-TiO_2. In Figure 10 I−V curves are shown for TiO_2 films with a thickness of 340 (A) and 1780 nm (B), respectively. It can be seen that in the dark the 340-nm film shows a symmetrical curve (I), although not completely linear. The 1780-nm film shows diode-type behavior (V). If illuminated, both samples show an increase in slope at 0V (II and VI), which is equivalent to a decrease in resistance. This is caused by the light-induced formation of electrons and holes in the P3OT (photoconductivity). The UV light is filtered out to prevent TiO_2 from beingoptically excited. Upon heating of the samples kept in air and in darkness, even steeper curves are measured (III, IV, and VII), indicating that the resistance of the heated films decreases. This is ascribed to the temperature dependence of the specific resistance of poly(3-octyl)thiophene. From the I−V curves measured in the dark it can be concluded that for the 340-nm thick film the P3OT penetrates all the way to the bottom and touches the TCO electrode. For the 1780-nm thick film this is not possible and at some location in the film interpenetration ends, which excludes contact between the TCO electrode and P3OT. Note that we cannot distinguish between complete and incomplete pore filling, as only information on how deep the P3OT penetrates the nanoporous TiO_2 is obtained. The change of the slope, if the samples are illuminated or heated, reveals that the resistance clearly originates from the

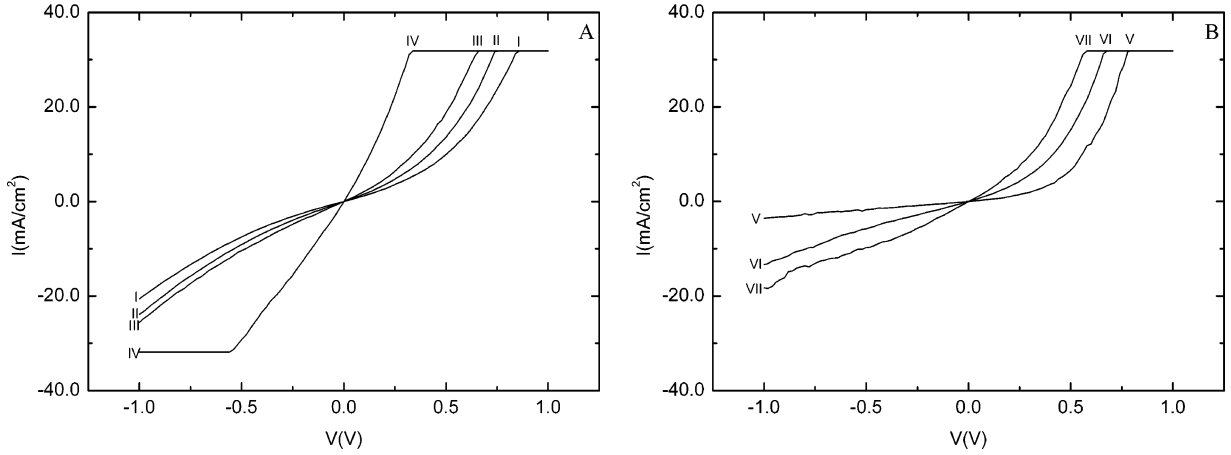

Figure 10. I−V curves for TCO/nc-TiO_2/P3OT/Au with two different thicknesses of the nc-TiO_2 film. The concentration of spin-coated P3OT is 10 mg/mL in chloroform, which leads to a film with the same optical density (OD) as an equivalent film of 60 nm deposited on a flat substrate. The slope of the curve at 0 V is taken as the reciprocal of the resistance of the TiO_2/P3OT combination. (A) Film thickness of nc-TiO_2 is 340 nm. I: measured in dark, $R = 2750\Omega$. II: measured under illumination (white light, 100 mW/cm^2, 400-nm high pass filter to remove UV-light), $R = 2130\Omega$. III: measured in dark, heated with hot air to about 40 °C, $R = 1630\Omega$. IV: measured in dark, heated by hot air to about 60 °C, $R = 450\Omega$. (B) Film thickness of nc-TiO_2 is 1870 nm. V: measured in dark, $R = 8350\Omega$. VI: measured under white light illumination (1000 W/m^2, 400-nm high pass filter to remove UV-light), $R = 2520\Omega$. VII: measured in dark, heated to about 40 °C, $R = 1370\Omega$.

P3OT film inside the TiO_2 pores and excludes pinholes or short-circuiting being the reason for the symmetrical or linear I−V curves.

The current−voltage measurements without selective TiO_2 contacts are repeated for different layer thicknesses of the nc-TiO_2 film and the resistance is calculated from the slope of the I−V curves at zero volts. All curves are recorded in the dark. For nc-TiO_2 films of 200 nm to around 1 μm the I−V curves show a straight or symmetrical line with a resistance around 1000 Ω (not shown). If the film thickness increases beyond approximately 1 μm, the shape of the I−V curves changes from linear/symmetrical to a more diode-like type of curve. The resistances increase to values of around 10 kΩ. From this we conclude that the maximum penetration depth of P3OT in this system is approximately 1 μm. This matches very well with the maximum of the short-circuit current, which occurs also for 1-μm thick films as shown in Figure 7B. In general, it is expected that the maximum penetration depth depends on of the concentration of the spin-coated P3OT solution, the amount of spin-coated material, and the spin-coat method (for example, whether multiple coatings are applied), and the pore size of the TiO_2 films. The influence of the latter parameters is studied by performing the same experiment with titanium dioxide powder of different particle sizes. In the case of 50-nm particles (prepared using a sol−gel method) the pore size is larger than that for the aerosol-synthesized TiO_2 as confirmed by SEM (not shown). For both the 50-nm and the 2-μm thick samples the I−V curve showed ohmic behavior, indicating that the P3OT reached all the way to the TCO electrode. The maximum penetration depth for this system is, therefore, substantially larger than that for the aerosol-synthesized TiO_2. For commercial 9-nm particles (Solaronix HT) the pore size is around 10 nm. For both 300-nm and 1-μm thick samples the I−V curve shows diode-type behavior, indicating that the P3OT does not penetrate all the way to the TCO contact. The maximum penetration depth for this system is, therefore, substantially less than that for the aerosol-synthesized TiO_2.

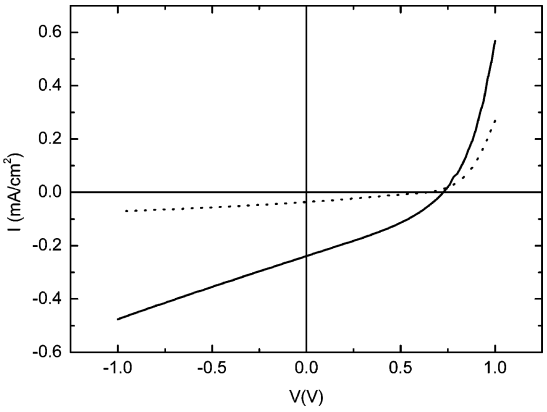

Figure 11. I−V curve for TCO/TiO_2 (70 nm)/nc-TiO_2/P3OT/Au. The nanocrystalline TiO_2 layer is 1 μm thick and consists of 50-nm particles. The dotted curve is a current−voltage graph of TCO/TiO_2 (70 nm)/P3OT/Au. Illumination with white light (100 mW/cm^2, not AM 1.5) takes place through the tin dioxide electrode, and a 400-nm high pass filter is used to prevent excitation of the TiO_2.

Figure 11 shows the current−voltage response for a 1-μm thick film of aerosol-synthesized anatase TiO_2 with interpenetrating P3OT (10 mg/mL). Also a current−voltage curve is shown for a solar cell comprising a flat dense TiO_2 layer (70 nm) with an equal amount of P3OT spin-coated on top (dotted curve). Although the light source is not AM 1.5 calibrated, the fill factor and efficiency can be determined to provide an indication of the cell performance. The values for the nanostructured cell are $I_{sc} = 0.25$ mA/cm^2, $V_{oc} = 0.72$ V, FF = 0.35, and $\eta = 0.06\%$, and for the flat cell are $I_{sc} = 37$ μA/cm^2, $V_{oc} = 0.66$ V, FF = 0.25, and $\eta = 0.003\%$. The nanostructured cell has a 20× higher efficiency than the flat cell. The photocurrent is linearly dependent on the irradiation intensity between 0.1 and 200 mW/cm^2. If the cells are kept in the dark at room temperature or at elevated temperatures (100 °C), the photovoltaic characteristics

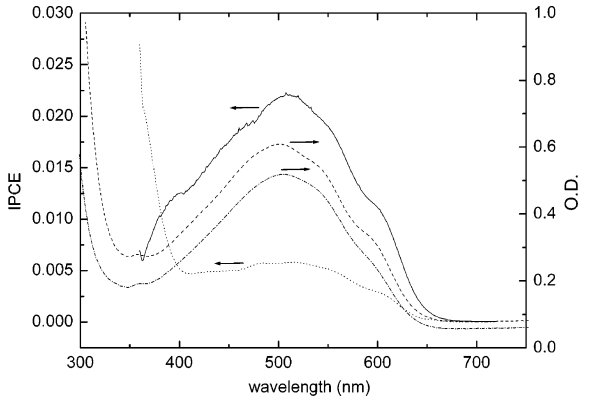

Figure 12. IPCE curve for TCO/TiO_2 (70 nm)/nc-TiO_2/P3OT/Au (solid line). The nanocrystaline TiO_2 layer is 1 μm thick and consists of 50-nm particles. The dotted curve is an IPCE plot of TCO/TiO_2 (70 nm)/P3OT/Au. The dashed curve is the absorption spectrum for the nanostructured cell and the dashed−dotted curve is the absorption curve for the flat cell. Illumination with monochromatic light (around 1 mW/cm^2) takes place through the tin dioxide electrode, and a 360-nm high pass filter is used.

are stable for several weeks. If illuminated continuously, the photocurrent decreases slightly at a time scale of a few hours indicating that photodegradation is occurring. This process is irreversible.

In Figure 12 the wavelength-dependent photocurrent spectra for these same cells are shown, converted to the incident photon to current efficiency (IPCE), together with the absorption spectra. The IPCE curve matches the shape of the absorption spectrum. The ODs of the nanostructured and flat cell are comparable, showing that indeed an amount of polymer similar to a flat film of 60 nm is penetrated inside the nc-TiO_2. When we estimate the nc-TiO_2 film to be around 50% porous (as for the TiO_2 in dye-sensitized cells[1]), a pore filling of slightly more than 10% is estimated.

Gebeyehu et al.[15,45] have reported on similar cells, using poly(3-octyl)thiophene spin-coated on top of 2-μm thick films consisting of 13-nm particles of anatase TiO_2. These cells have an efficiency of 0.08% under solar simulated white light of 80 mW/cm^2. When Ru 535-dye (cis-[$L_2Ru(SCN)_2$] in which L is 2,2′-dipyridine-4,4′-dicarboxylic acid) is applied between TiO_2 and polymer, as in dye-sensitized solar cells,[2] the efficiency becomes twice as high. The Ru-dye absorbs visible light and injects electrons very efficiently into the TiO_2 network. The P3OT has a double function: light-absorption/carrier injection and hole conduction. Still, these efficiencies are small compared to cells functioning with a liquid electrolyte. Gebeyehu et al. remark that the limiting step for these devices is probably the hole transfer from the Ru-dye to the polymer, because injection of electrons from the Ru-dye to TiO_2 is expected to be very fast and there is sufficient hole transport in the polymer. In the present study the transport of excitons to the TiO_2 particle surface is probably also a bottleneck of the device. Nevertheless, the area enlargement is effective, as nanostructured cells exhibit a remarkable efficiency enhancement of a factor of 20 compared to that of bi-layer devices.

(45) Gebeyehu, D.; Brabec, C. J.; Saricifici, N. S.; Vangeneugden, D.; Kiebooms, R.; Vanderzande, D.; Kienberger, F.; Schindler, H. *Synth. Met.* **2002**, *125*, 279−287.

Conclusions

Using an aerosol synthesis route, thin films of nanocrystalline, stoichiometric anatase titanium dioxide are deposited. The minimum size of the particles is 50 nm; at higher concentrations and carrier gas flows agglomeration occurs. The growth rate is linearly dependent on the flow rate of the carrier gas. Spin-coating poly(3-octyl)thiophene on top of these TiO_2 films leads to solar cells, which show efficiencies 20 times higher than that of cells with "flat" TiO_2. Maximum photocurrents are obtained for cells with 1-μm thick TiO_2 films consisting of 50-nm particles. These cells exhibit a short circuit current of 0.25 mA/cm^2, an open circuit voltage of 0.72 V, a fill factor of 0.35, and an overall efficiency of 0.06%. The IPCE is 2.5% at 488 nm. Devices for which the P3OT is spin-coated during TiO_2 deposition show similar efficiencies, indicating that the penetration of the P3OT in the porous TiO_2 network is quite effective. By analysis of current−voltage characteristics of intermixing layers of aerosol-synthesized TiO_2 and P3OT (10 mg/mL in chloroform), sandwiched between two electrodes, we have found that the maximum penetration depth of P3OT inside the nanoporous TiO_2 is around 1 μm. Larger pore sizes facilitate penetration of P3OT, but because of the small exciton diffusion length more recombination occurs. Interpenetrating solar cells with polymers and TiO_2 will be a tradeoff between pore-filling ability and recombination losses. An increase of the amount of P3OT in the pores will probably increase the efficiency. We have shown that it is possible to make interpenetrating networks of TiO_2 and P3OT both in one and in two steps, but an increase in efficiency is demanded before practical application of these kinds of cells comes into view.

Acknowledgment. We are grateful to Han Kiersch of the Department of Material Science, Surface Science Group for assistance with the HRSEM measurements. We also thank the Energy Research Centre of The Netherlands (ECN) for preparing a paste of 50-nm TiO_2 particles. Dr. Louis Winnubst (Twente University) is acknowledged for valuable discussions. The investigations were co-financed by The Netherlands Agency for Energy and the Environment (NOVEM).

CM031099M